Published in final edited form as:
Cell. 2014 April 10; 157(2): 486–498. doi:10.1016/j.cell.2014.01.065.

Activity-Dependent p25 Generation Regulates Synaptic Plasticity and Aβ-Induced Cognitive Impairment

Jinsoo Seo[1,2], **Paola Giusti-Rodríguez**[1,2,5], **Ying Zhou**[1,2], **Andrii Rudenko**[1,2], **Sukhee Cho**[1,2], **Kristie T. Ota**[1,2,6], **Christine Park**[1,2], **Holger Patzke**[1,2,7], **Ram Madabhushi**[1,2], **Ling Pan**[1,2], **Alison E. Mungenast**[1,2], **Ji-Song Guan**[1,2,8], **Ivana Delalle**[3], and **Li-Huei Tsai**[1,2,4,*]

[1]The Picower Institute for Learning and Memory, Cambridge, MA 02139, USA

[2]Department of Brain and Cognitive Sciences Massachusetts Institute of Technology, Cambridge, MA 02139, USA

[3]Department of Pathology and Laboratory Medicine, Boston University School of Medicine, Boston, MA 02118, USA

[4]Broad Institute of Harvard University and Massachusetts Institute of Technology, Cambridge, MA 02142, USA

SUMMARY

Cyclin-dependent kinase 5 regulates numerous neuronal functions with its activator, p35. Under neurotoxic conditions, p35 undergoes proteolytic cleavage to liberate p25, which has been implicated in various neurodegenerative diseases. Here, we show that p25 is generated following neuronal activity under physiological conditions in a GluN2B- and CaMKIIα-dependent manner. Moreover, we developed a knockin mouse model in which endogenous p35 is replaced with a calpain-resistant mutant p35 (Δp35KI) to prevent p25 generation. The Δp35KI mice exhibit impaired long-term depression and defective memory extinction, likely mediated through persistent GluA1 phosphorylation at Ser845. Finally, crossing the Δp35KI mice with the 5XFAD mouse model of Alzheimer's disease (AD) resulted in an amelioration of β-amyloid (Aβ)-induced synaptic depression and cognitive impairment. Together, these results reveal a physiological role of p25 production in synaptic plasticity and memory and provide new insights into the function of p25 in Aβ-associated neurotoxicity and AD-like pathology.

*Correspondence: lhtsai@mit.edu.
[5]Present address: University of North Carolina at Chapel Hill, Chapel Hill, NC 27599, USA
[6]Present address: Laboratory of Molecular Psychiatry, Yale University School of Medicine, New Haven, CT 06508, USA
[7]Present address: EnVivo Pharmaceuticals, 500 Arsenal Street, Watertown, MA 02472, USA
[8]Present address: School for Lifescience, Tsinghua University, Beijing 10006, China

SUPPLEMENTAL INFORMATION

Supplemental Information includes Extended Experimental Procedures, seven figures, and two tables and can be found with this article online at http://dx.doi.org/10.1016/j.cell.2014.01.065.

INTRODUCTION

Cyclin-dependent kinase 5 (Cdk5) is a multifaceted serine/threonine kinase that plays essential roles in various aspects of brain development, including neuronal migration and positioning (Chae et al., 1997; Gilmore et al., 1998), and dendritic spine formation (Fu et al., 2007; Kim et al., 2006). In addition, Cdk5 phosphorylates a number of substrates at the presynaptic and postsynaptic terminals of mature neurons, and mediates various synaptic functions (Su and Tsai, 2011). Thus, the mechanisms by which Cdk5 activity is regulated to mediate these functions deserve serious attention.

Conventionally, Cdk5 activity is thought to be governed by its binding to its regulatory subunits p35 or p39, and mice simultaneously deficient in both p35 and p39 recapitulate the phenotypes of Cdk5 null mice (Ko et al., 2001). Interestingly, Cdk5 is also activated through its association with p25, a proteolytic fragment of p35 that is generated via its cleavage by calpain, a calcium-dependent cysteine protease. p25 has a longer half-life and a more diffuse subcellular distribution than p35 (because the myristoylated portion of p35 resides in the cleaved portion) (Patrick et al., 1999), and confers p25/Cdk5 with distinct properties compared with p35/Cdk5. Elevated levels of p25 have been documented upon exposure to various neurotoxic stimuli, including oxidative stress and β-amyloid (Aβ) peptides (Lee et al., 2000b), and in the brain of multiple Alzheimer's disease (AD) mouse models (Crews et al., 2011; Oakley et al., 2006; Otth et al., 2002). An increase in p25 levels in postmortem AD brains has also been reported (Patrick et al., 1999; Sadleir and Vassar, 2012; Swatton et al., 2004), although other studies detected no such differences (Engmann et al., 2011; Tandon et al., 2003; Yoo and Lubec, 2001). In addition, transgenic mice that overexpress p25 exhibit various features of neurotoxicity, such as tau pathology, Aβ accumulation, astrogliosis, and profound memory impairment (Su and Tsai, 2011). In contrast, transgenic mice with milder p25 overexpression exhibit improved memory function (Angelo et al., 2003). Together, these observations suggest that p25 leads to aberrant Cdk5 activity that contributes to neurode-generation. However, it remains to be determined whether p25 generation is restricted to pathological conditions or is also important for physiological neuronal functions. Furthermore, despite the elevation in p25 levels that occurs under various neurotoxic conditions, the specific contribution of p25, if any, to AD-like pathologies, including cognitive impairment, remain obscure.

RESULTS

Neuronal Activity Regulates p25 Generation

To address whether p25 is generated under physiological conditions, we treated cultured primary neurons with either N-methyl-D-aspartate (NMDA) to induce chemical long-term depression (LTD) (Lee et al., 1998) or glycine to induce chemical long-term potentiation (LTP) (Lu et al., 2001). p25 generation was evident as early as 5 min following treatment and persisted for more than 30 min (Figure 1A). In addition, acute hippocampal slices from wild-type (WT) mice showed a nearly 2-fold increase in p25 levels following glycine or NMDA treatment (Figure 1B). To determine whether p25 is produced following hippocampus-dependent learning, we harvested hippocampal tissue following contextual fear conditioning (FC) training, and observed markedly increased p25 levels in the FC group

compared with the naive group (Figure 1C). In addition, reexposure to the training chamber 24 hr after the training increased p25 levels (Figure S1A available online). These results indicate that p25 is generated in the brain in an activity-dependent manner.

p35 Is Cleaved by Calpain in an NMDAR- and CaMKIIα-Dependent Manner

In an effort to elaborate the mechanisms that lead to p25 generation, we first used calpeptin to inhibit calpain, which cleaves p35 to p25 following neurotoxic stimuli. NMDA treatment of acute hippocampal slices in the presence of calpeptin substantially reduced p25 levels, suggesting that calpain is required for activity-dependent p25 liberation (Figure 1D). Next, we blocked α-amino-3-hydroxy-5-methyl-4-isoxazolepropionic acid receptors (AMPARs) and NMDA receptors (NMDARs), which mainly govern postsynaptic Ca^{2+} influx under physiological conditions (Collingridge et al., 2004). Incubation with the NMDAR antagonist APV, but not the AMPAR antagonist CNQX, severely diminished NMDA-induced p25 generation (Figure 1D). In addition, inhibition of GluN2B, but not GluN2A (using ifenprodil and NVP-AAM077, respectively), also led to reduced p25 levels (Figure 1D). The Ca^{2+}/calmodulin kinase CaMKIIα, which plays a prominent role in synaptic plasticity and memory formation, interacts with p35 in a Ca^{2+}- and NMDAR-dependent manner (Dhavan et al., 2002). Prompted by these observations, we treated acute hippocampal slices with the specific CaMKIIα inhibitor, KN-62, and showed that this was sufficient to abolish NMDA-induced p25 generation (Figure 1D). Finally, immunoprecipitation (IP) experiments revealed that both CaMKIIα and GluN2B interact with p35 in a complex that also contains calpain 1 at the hippocampal postsynaptic density (PSD) (Figures 1E and S1B). Together, these results suggest a signaling cascade in which activation of NMDAR stimulates calpain-mediated p35 cleavage and the liberation of p25 from PSD (Figure S1C) in a GluN2B- and CaMKIIα-dependent manner.

Generation of Cleavage-Resistant p35 Knockin Mice

To determine whether activity-induced p25 production plays a physiological role, we developed a calpain cleavage-resistant p35 protein in which six amino acid residues adjacent to the calpain-cleavage site (Δ93–98; Lee et al., 2000b) were deleted and the Ala residue at the cleavage site was replaced with Leu (Figure 2A). The cleavage resistance of the mutant p35 (Δp35) was first verified in human neuroblastoma cells treated with ionomycin, a calcium ionophore (Figure S2A). Notably, Δp35 showed no differences in half-life, subcellular localization, or capacity to activate Cdk5 compared with WT p35 (Figures S2B–S2D), indicating that the cleavage resistance of the Δp35 protein is successfully endowed without altering other characteristics of native p35.

Given these properties of Δp35 in vitro, we developed a knockin mouse in which the endogenous p35 is replaced with Δp35 (Δp35KI; Figure S2E). The Δp35KI mice are viable and fertile, and devoid of neurodevelopmental abnormalities (Figure S3A). The expression levels of Δp35 were similar to those of p35 in brain lysates from WT mice, and Cdk5 activity was comparable between the two groups (Figures 2B and 2C). Importantly, there was no detectable p25 immunoreactivity in hippocampal slices from Δp35KI mice following NMDA or glycine treatment (Figure 2D), indicating that activity-dependent p25 generation is absent in Δp35KI mice.

Δp35KI Mice Exhibit Normal Learning but Impaired Memory Extinction

To investigate the role of activity-induced p25 generation in vivo, we first performed a series of behavioral assays. An assessment of overall exploratory activity in the open field test and anxiety in the light-dark exploration test revealed no differences between Δp35KI and WT mice (Figures S3B–S3H). We then performed contextual FC to assess associative learning in the Δp35KI mice. There was no significant difference in animal movement in the conditioning chamber during the habituation period between the two groups (Figure 2E). During the context-dependent memory test, the freezing behavior of Δp35KI mice was comparable to that of WT mice, indicating normal associative memory formation in the Δp35KI mice (day 2, Figure 2F). Surprisingly, however, Δp35KI mice showed significantly higher levels of freezing behavior on subsequent trials, indicative of impaired memory extinction (Figure 2F). To further characterize this memory phenotype, we employed the Morris water maze test. We trained mice in the water maze for 8 days, and conducted probe tests on three consecutive days in order to examine their extinction phenotype (Zhang et al., 2011). WT and Δp35KI mice were similar in measures of swim speed, latency in locating the platform, and the number of platform crossings during the first probe trial, indicating no differences in either learning or spatial memory (Figures 2G–2I). Probe trials repeated on subsequent days induced memory extinction in WT mice, as evidenced by a significant decrease in the number of platform crossings (Figure 2J), as well as a similar decrease in amount of time spent in the target quadrants on probe trial days 2 and 3 (Figure 2K). In contrast, the Δp35KI mice showed increased crossing of the platform location (Figure 2J) and continued to preferentially explore the target quadrant during additional probe trials (Figure 2K). Altogether, these data strongly suggest a role for p25 in memory extinction.

Δp35KI Mice Exhibit Normal Hippocampal LTP but Impaired NMDAR-Dependent LTD

We next addressed the role of p25 generation in synaptic function by performing extracellular and intracellular recordings in acute hippocampal slices from Δp35KI and WT mice. An examination of the basal synaptic transmission (Figure 3A) and the probability of presynaptic neurotransmitter release (as determined by measuring paired-pulse facilitation (PPF) ratios; Figure 3B) revealed no differences between Δp35KI and WT slices. Similarly, whole-cell recordings of CA1 pyramidal neurons showed no significant differences in either the frequency or amplitude of miniature excitatory postsynaptic currents (mEPSCs) or miniature inhibitory PSCs (mIPSCs) between Δp35KI and WT slices (Figures 3C and 3D). Next, we investigated synaptic plasticity at Schaffer collateral-CA1 synapses. In Δp35KI hippocampal slices, LTP induced by theta-burst stimulation (TBS) was comparable to WT levels (Figure 3E). However, the induction of NMDAR-dependent LTD by single-pulse low-frequency stimulation (SP-LFS) was significantly impaired in the Δp35KI mice (Figure 3F). We observed normal metabotropic glutamate receptor (mGluR)-dependent LTD in Δp35KI hippo-campal slices (Figure S4A). Furthermore, mGluR activation did not induce p25 generation in WT hippocampus (Figure S4B). These results indicate that activity-induced p25 is necessary for NMDAR-dependent LTD at hippocampal synapses.

p25/Cdk5 Regulates AMPAR Endocytosis via PP1, Calcineurin, and DARPP-32

Memory extinction and NMDAR-dependent LTD both require AMPAR endocytosis, which is mediated by phosphatase-dependent AMPAR dephosphorylation (Dalton et al., 2008; Kim et al., 2007; Lee et al., 2000a). From our results thus far, we reasoned that the p25/Cdk5 kinase might play a role in LTD by facilitating AMPAR endocytosis. This was indeed shown to be the case. First, a comparison of Cdk5 activity following NMDA treatment revealed increased Cdk5 activity in hippocampal slices from WT, but not Δp35KI, mice (Figure 4A), suggesting that NMDA-induced p25 generation increases Cdk5 activity in the hippocampus. AMPAR endocytosis during LTD is associated with the phosphorylation of GluA1 at Ser845 and changes in GluA1 surface levels (Lee et al., 2000a). Whereas NMDA administration induced a robust reduction in GluA1 phospho-(p)Ser845 and surface GluA1 levels in WT hippocampal slices, no such changes were detected following NMDA treatment of Δp35KI slices (Figure 4B). These results suggest that p25/Cdk5 activity is essential for AMPAR dephosphorylation and endocytosis.

To further delineate the mechanisms underlying this process, we focused on two protein phosphatases that mediate AMPAR dephosphorylation during LTD formation: protein phosphatase-1 (PP1) and calcineurin (PP2B) (Mulkey et al., 1993, 1994). Although there was no difference in the levels of PP1 and calcineurin either basally or following NMDA treatment between WT and Δp35KI hippocampus (Figure 4D and data not shown), phosphatase assays revealed that NMDA administration significantly increased the activity of both PP1 and calcineurin in WT, but not Δp35KI, hippocampus (Figure 4E). To test whether the inhibition of p25 generation alters NMDAR-dependent calcium influx, we conducted calcium imaging in primary cultured neurons from WT or Δp35KI mice. We observed no differences in NMDA-induced intracellular calcium changes between the two groups (Figure S4C), suggesting that the impaired calcineurin activation evident in the Δp35KI mice is unlikely to result from altered NMDAR-dependent calcium influx.

The dopamine and cyclic AMP-regulated phosphoprotein DARPP-32 is a well-established negative regulator of PP1 in the dopaminergic system (Hemmings et al., 1984). Phosphorylation at Thr34 by protein kinase A (PKA) activates DARPP-32, whereas calcineurin dephosphorylates this residue (Halpain et al., 1990). Interestingly, Cdk5 is known to phosphorylate DARPP-32 at Thr75 and block its activation (Bibb et al., 1999). Thus, we speculated that p25/Cdk5 might regulate DARPP-32 and, in turn, PP1 activity in the hippocampus. We first confirmed that DARPP-32 is expressed in the hippocampus, and found that its levels were comparable between Δp35KI and WT mice (Figure S4D). Interestingly, the Cdk5f/f/T29 mouse, in which Cdk5 is deleted in CA1 (Guan et al., 2011), exhibits markedly reduced levels of DARPP-32 pThr75 in this region (Figure 4F), suggesting that DARPP-32 is a Cdk5 substrate in the hippocampus. Next, we found that NMDA administration caused a signifi-cant upregulation of DARPP-32 pThr75 in WT hippocampal slices, whereas no such changes were detectable in the Δp35KI hippocampus (Figure 4G). Taken together, these results unveil a novel physiological function for p25/Cdk5 in AMPAR endocytosis that is likely mediated through its inhibition of DARPP-32 and the activation of PP1 and calcineurin in response to neuronal activation.

p25/Cdk5 Regulates Aβ-Induced Synaptic Depression in the Hippocampus

Many lines of evidence indicate that Ab increases intracellular Ca^{2+} levels and subsequently induces hippocampal synaptic depression via the activity of GluN2B and calcineurin (Kamenetz et al., 2003; Kuchibhotla et al., 2008; Li et al., 2011). It has also been reported that incubation of cultured neurons with Ab induces p25 generation (Lee et al., 2000b; Yang et al., 2008) and that p25 levels are upregulated in familial AD mouse models (Crews et al., 2011; Oakley et al., 2006; Otth et al., 2002). We showed that p25 generation impacts memory extinction and synaptic plasticity under physiological conditions; thus, we reasoned that a chronic upregulation of p25 in response to toxic stimuli might dysregulate these processes. To test whether p25 plays a role in Aβ-induced synaptic depression, we examined oligomeric $Aβ_{1-42}$-induced synaptic depression in hippocampal slices from Δp35KI and WT mice. As previously reported (Kamenetz et al., 2003), incubation of hippocampal slices in Aβ gradually reduced the field excitatory postsynaptic potential (fEPSP) slope in the WT slices. In contrast, no such changes were detectable in Δp35KI hippocampal slices (Figure 5A). Additionally, we verified that Aβ treatment increased p25 levels in hippocampal slices from WT, but not Δp35KI, mice (Figure 5B). Thus, p25 generation is essential for Aβ-induced synaptic depression in the hippocampus.

p25-Mediated DARPP-32 Inhibition and AMPAR Dephosphorylation Are Observed in the 5XFAD Mouse

The resistance to Aβ-induced synaptic depression apparent in the Δp35KI mice led us to question whether p25/Cdk5 activity mediates synaptic dysfunction in the brain of an AD mouse model that is characterized by Aβ deposition. We crossed the Δp35KI mouse with the 5XFAD mouse, a well-established model that harbors three amyloid precursor protein (APP) and two presenilin 1 (PSEN1) mutations that are causally linked to familial AD (Oakley et al., 2006). Hippocampal lysates from 5XFAD mice showed increased Cdk5 activity compared with either WT or Δp35KI mice. In contrast, Cdk5 activity was significantly attenuated in the 5XFAD;Δp35KI compound mice, suggesting that the elevation of Cdk5 activity in the 5XFAD hippocampus is p25 dependent (Figure 5C). From our previous observations, we hypothesized that alterations in p25/Cdk5-mediated DARPP-32 phosphorylation and AMPAR endocytosis may contribute to the synaptic defects that accrue in 5XFAD brains. Interestingly, we observed increased levels of DARPP-32 pThr75 and decreased GluA1 pSer845 levels in 5XFAD hippocampus compared with either WT or Δp35KI mice. However, consistent with attenuated Cdk5 activity, the levels of DARPP-32 pThr75 and GluA1 pSer845 in 5XFAD;Δp35KI hippocampus were comparable to those in WT and Δp35KI mice (Figures 5D and 5E). Fibrillar Aβ deposition in the hippocampus of 5XFAD mice becomes apparent at 3–4 months of age (Oakley et al., 2006; Figure S5A). To address whether DARPP-32 and GluA1 phosphorylation are altered prior to Aβ deposition in hippocampus, we examined hippocampi from 2-month-old WT, 5XFAD, Δp35KI, and 5XFAD;Δp35KI mice, and found no differences in either the DARPP-32 pThr75 or GluA1 pSer845 levels (Figure S5B). Interestingly, the p25 levels in the hippocampi of 5XFAD mice were comparable to those in the WT at this age. Altogether, these data suggest that Aβ deposition induces p25 generation and leads to DARPP-32 inhibition and GluA1 Ser845 dephosphorylation.

Blockade of p25 Generation Rescues Synaptic Dysfunction and Cognitive Impairment in 5XFAD Mice

To further determine the contribution of aberrant p25 generation to synaptic dysfunction and cognitive impairment in the 5XFAD mice, we examined synaptic physiology at Schaffer collateral-CA1 synapses. We observed reduced input-output ratios in both 5XFAD and 5XFAD;Δp35KI hippocampi compared with either WT or Δp35KI mice (Figure S6A), indicating a decreased basal synaptic transmission phenotype in these mice that is not altered by the absence of p25. We previously showed that excessive GluA1 Ser845 dephosphorylation in the 5XFAD hippo-campus, associated with decreased surface levels of AMPARs, is attenuated in 5XFAD;Δp35KI compound mice (Figure 5E); thus, it is possible that other factors may underlie impaired basal synaptic transmission in the 5XFAD mice in a p25-independent manner. However, we found that the impaired LTP that is characteristic of the 5XFAD hippocampus (Chen et al., 2012; Kimura and Ohno, 2009) was restored to WT levels in the 5XFAD;Δp35KI compound mice (Figure 6A). Similarly, in behavioral experiments, we found that the established 5XFAD phenotypes of reduced anxiety (Jawhar et al., 2012) and poor cognitive performance in the novel-object recognition and contextual and cued FC paradigms were all suppressed in 5XFAD;Δp35KI compound mice (Figures 6B and 6C, and S6C).

p25 Inhibition Attenuates HDAC2 Upregulation, Glial Activation, and Aβ Accumulation in the 5XFAD Mouse Brain

Our results prompted us to determine the specific effects of Aβ-induced p25 generation on various pathological hallmarks of AD. Histone deacetylase 2 (HDAC2) is a Class I HDAC that negatively regulates the expression of genes associated with learning and memory (Guan et al., 2009), which we previously reported to be a negative regulator of learning and memory that is induced upon aberrant Cdk5 activity and in the AD brain (Gräff et al., 2012). Whereas elevated HDAC2 levels and a concomitant decrease in histone H3 acetylation at Lys 9/14 (AcH3; H3K9/14) were detected in CA1 of 6-month-old 5XFAD mice, these changes were significantly attenuated in 5XFAD;Δp35KI mice (Figure 7A).

Similarly, an increase in reactive astrocytes and activated microglia in the 5XFAD mice hippocampus, a major pathological feature of the AD brain (Perry et al., 2010; Verkhratsky et al., 2010), was attenuated in the 5XFAD;Δp35KI mice (Figures 7B and 7C). Moreover, although the mRNA levels of cytokines or chemokines such as *TNF-α*, *Il-1ν*, and *MIP-1α* were elevated in the 5XFAD mice, they were significantly reduced in the 5XFAD;Δp35KI mice (Figure S7A). These results suggest that p25 generation contributes substantially to these AD-related pathologies.

In this work, we observed that Aβ stimulates the accumulation of p25; however, the formation of p25 is also known to upregu-late β-secretase 1 (BACE1) (Cruz et al., 2006; Wen et al., 2008). An upregulation of BACE1 in 5XFAD mice was reported previously (Zhao et al., 2007). This increase in BACE1 levels in the 5XFAD brain was suppressed in the absence of p25 generation in 5XFAD;Δp35KI mice (Figure 7D). Finally, we observed modest but significant reductions in plaque load and size in the hippocampus of 5XFAD;Δp35KI mice compared with 5XFAD mice (Figure 7E). Furthermore, the levels of

$A\beta_{1-42}$ and $A\beta_{1-40}$ were reduced by 20%–30% in the hippocampus of 5XFAD; Δp35KI mice compared with 5XFAD mice (Figure 7F).

DISCUSSION

In this study, our use of a mouse model that specifically precludes the generation of the Cdk5-activating peptide, p25, allowed us to delineate both the physiological and pathological consequences of p25 generation. Our results show that p25 functions as an integral component of synaptic plasticity, and that blockade of p25 generation impairs hippocampal LTD and memory extinction. Furthermore, we provide multiple lines of evidence demonstrating that chronic p25 generation caused by Aβ induces persistent synaptic depression, impaired synaptic plasticity, and reduced cognitive capacity, and thereby contributes to the development of AD-like pathologies.

Activity-Induced p25 Regulates LTD and Memory Extinction

We show that diverse physiological stimuli and learning tasks induce p25 formation in a GluN2B- and CaMKIIα-dependent manner, and that activity-induced p25/Cdk5 specifically mediates hippocampal LTD, but not LTP. These findings are consistent with the observation that p35-deficient mice display normal LTP but impaired LTD at hippocampal synapses (Ohshima et al., 2005). Interestingly, p25 generation and elevated Cdk5 activity were also detected following glycine-induced chemical LTP in hippocampal slices from WT mice, and a similar increase in Cdk5 activity was observed in the absence of p25 generation in Δp35KI mice (Figure 1B and data not shown). These observations, together with the findings of normal LTP in the Δp35KI hippocampus (Figure 3E), indicate that p25 production may not be necessary for this form of synaptic plasticity. Perhaps this kind of stimulation increases the interaction of Cdk5 and p35 (Dhavan et al., 2002), or increases Cdk5 phosphorylation at Tyr15 (Zukerberg et al., 2000), which upregulates Cdk5 activity independently of p25 generation. Nevertheless, it is interesting that p25 generation is induced by LTP protocols but is not involved in LTP induction. Memory extinction has been often considered to involve a decay of preexisting memory, caused by the degradation of memory-related molecules (Lee et al., 2008). However, recent studies have raised the possibility that extinction could be an active process that is mediated by molecules induced during learning processes (Shuai et al., 2010; Tronson et al., 2012). Interestingly, inhibition of either NMDARs or CaMKIIα in the hippocampus was shown to impair the extinction of conditioned fear memory (Szapiro et al., 2003). Consistent with these findings, blocking p25 generation specifically impairs memory extinction, but not memory acquisition itself (Figures 2F, 2J, and 2K). Thus, learning-induced p25 is specifically required for extinction learning.

p25/Cdk5 Regulates NMDA-Induced AMPAR Endocytosis by Inhibiting DARPP-32 and Activating Calcineurin in the Hippocampus

We show that the blockade of p25 generation compromises NMDA-induced AMPAR dephosphorylation and subsequent AMPAR endocytosis (Figures 4B and 4C). It is known that activation of NMDARs negatively impacts DARPP-32 by inducing its dephosphorylation in the striatum (Halpain et al., 1990). Here, we identify DARPP-32 as the

relevant Cdk5 substrate in the hippocampus (Figure 4F). We show that p25/Cdk5 phosphorylates DARPP-32 at Thr75 following NMDA treatment (Figure 4G), which correlates with an increase in PP1 activity (Figure 4E), although we cannot rule out the possibility that other PP1 inhibitor proteins, such as PP1 inhibitor-1, could also be regulated by p25/Cdk5, as previously speculated (Etkin et al., 2006). In addition to the regulation of DARPP-32 and PP1 activity, calcineurin activation following NMDA treatment is also significantly impaired in the Δp35KI mouse hippocampus (Figure 4E). It is presently unclear how activity-induced p25 regulates calcineurin activity at hippocampal synapses. Previous studies have shown that caspase-3 activity is increased by NMDAR activation, and that caspase-3 knockout mice display impaired hippocampal LTD but normal LTP (Li et al., 2010). Furthermore, it was shown that p25/Cdk5 increases caspase-3 activity (Cruz et al., 2003), and activated caspase-3 induces proteolytic cleavage of calcineurin, thereby increasing its catalytic activity (Mukerjee et al., 2000). In the AD mouse brain, increased caspase-3 activity leads to dephosphorylation of GluA1 Ser845 through the activation of calcineurin (D'Amelio et al., 2011). Importantly, Aβ-induced caspase-3 activation is significantly reduced in Δp35KI neurons compared with WT neurons (Figure S7B). These data suggest that p25/Cdk5 regulates calcineurin activity via caspase-3.

p25: A Link between Aβ and AD-Like Pathologies

Our study demonstrates that physiological neuronal activity results in the generation of p25 and that the resultant p25/Cdk5 is necessary for synaptic depression. As previously speculated (Kim and Ryan, 2010; Mitra et al., 2012; Seeburg et al., 2008), activation of Cdk5 by p25 under these conditions may constitute a homeostatic mechanism that is required to prevent hyperactivity in neuronal networks. Interestingly, a number of reports have described that neuronal activity correlates with Aβ production (Buckner et al., 2005; Cirrito et al., 2005; Kamenetz et al., 2003). It is also known that p25 overexpression increases Aβ levels in vivo through a mechanism involving BACE1 (Cruz et al., 2006; Wen et al., 2008). Together, these observations suggest that a feed-forward relationship may exist between p25 and Aβ generation, wherein activity-induced p25 generation not only participates in the maintenance of brain activity but also upregulates Aβ levels. These elevated Aβ levels then further increase p25.

p25/Cdk5 Contributes to Aβ-Induced Synaptic Depression and AD-Like Pathologies

A key finding of the current study is that Aβ-induced synaptic depression at hippocampal synapses is regulated by p25 (Figure 5A). It has been suggested that Aβ facilitates LTD by inhibiting glutamate uptake (Li et al., 2011). Interestingly, we observed increased p25 levels in WT hippocampal slices following inhibition of glutamate uptake (Figure S7C). Because of the adverse effects of p25 in neurons, many studies have focused on inhibiting p25 using Cdk5 antagonists or truncated peptides derived from p35 (Kesavapany et al., 2007; Su and Tsai, 2011). Although aberrant Cdk5 activity elicited by p25 may be suppressed under these conditions, it is unclear whether these effects are specific to p25/Cdk5, or whether p35/Cdk5 activity may also be affected. To delineate the precise role of p25/Cdk5 in a mouse model of AD, we took advantage of Δp35KI mice, thereby blocking the generation of p25 in 5XFAD mice, which were previously shown to exhibit elevated p25 levels at a relatively young age (Oakley et al., 2006). We show that the phenotypes of impaired LTP and cognitive deficits

were completely suppressed by blocking p25 production in these mice (Figures 6A–6C). Further, the increases in astrocyte and microglial activation, proinflammatory cytokines, and HDAC2 expression observed in the 5XFAD mice were markedly reduced in the absence of p25 accumulation (Figures 7A–7C and S7A). Finally, elevated levels of Aβ42/40, as well as BACE1, were reduced in the 5XFAD mice when p25 generation was blocked (Figures 7D and 7F). These results strongly support the notion that p25 accumulation plays an important role in AD pathogenesis and that inhibition of p25/Cdk5 can potentially mitigate AD-related pathologies and cognitive abnormalities.

EXPERIMENTAL PROCEDURES

See Extended Experimental Procedures for additional details regarding the materials and methods used in this work.

Animals

All experiments were performed according to the Guide for the Care and Use of Laboratory Animals and were approved by the National Institutes of Health and the Committee on Animal Care at the Massachusetts Institute of Technology. 5XFAD transgenic mice were obtained from The Jackson Laboratory.

Primary Neuronal Cultures

Cortical and hippocampal cultures were prepared from embryonic day 15 (E15) and E16 C57BL/6 mice, and experiments were performed at 14– 16 days in vitro (DIV).

Immunoblot Analysis

Primary neurons were lysed or hippocampus was homogenized, and the same quantities of lysates were subjected to SDS-PAGE and proved with the indicated antibodies. All of the antibodies used in this study are listed in Table S1.

CoIP Study

PSD fractions were prepared as previously described with some modifications (Carlin et al., 1980). IP from PSD fractions was performed by incubating the lysates with 1 mg of the indicated antibodies overnight at 4°C. Protein A sepharose beads were then added and allowed to rock for ~2 hr at 4°C. The beads were then washed three to five times and immunocomplexes were eluted by addition of sample buffer and boiling, and analyzed by SDS-PAGE.

DNA Constructs

All of the primers that were used to either generate or sequence constructs are listed in Table S2.

IP-Linked Cdk5 Kinase Assays

Whole hippocampus or NMDA/Gly-treated hippocampal slices were lysed and incubated with anti-Cdk5 antibody for 1 hr at 4°C. The active Cdk5 complex was isolated by

incubation with protein A sepharose beads, and then the immunoprecipitate was subjected to a Cdk5 kinase assay using histone H1 peptide (PKTPKKAKKL) as a substrate. Once a reaction mixture containing (mM) 20 MOPS (pH 7.2), 5 $MgCl_2$, 0.5 H1 peptide, 0.1 ATP, and 2.5 μCi γ-^{32}ATP was added, the reaction continued for 20 min at room temperature, and was halted by placing samples on ice for 5 min. Supernatants were spotted on P-cellulose discs, washed in 0.3% phosphoric acid, and counted in a liquid scintillation counter.

Generation of the Δp35-3xHA Knockin Mouse

For details regarding the generation of the Δp35-3xHA knockin mouse, see Extended Experimental Procedures.

Biotinylation Assay

Hippocampal slices were incubated in ice-cold artificial cerebrospinal fluid (ACSF) containing 2 mg/ml biotin (EZ-Link Sulfo-NHS-Biotin; Pierce) for 10 min, and then washed five times with Tris-buffered saline and homogenized with ice-cold IP buffer containing (mM) 20 Na_3PO_4, 150 NaCl, 10 EDTA, 10 EGTA, 10 $Na_4P_2O_7$, 50 NaF and 1 Na_3VO_4, and 1% Triton X-100 at pH 7.4. Lysates were mixed with Neutravidin slurry (1:1 in 1% Triton X-100 IPB) and rotated for 2 hr at 4°C. Some homogenates were used to measure the total GluA1 level. The Neutravidin beads were isolated by brief centrifugation at 1,000 × *g* and biotinylated surface proteins were eluted by addition of sample buffer and boiling, and analyzed by SDS-PAGE.

Protein Phosphatase Assay

Hippocampal lysates were immunoprecipitated with anti-PP1 or anti-calcineurin antibody overnight at 4°C, and then incubated with Protein A-Sepharose beads for another 2 hr. The immunoprecipitates were washed three times with lysis buffer, resuspended with assay buffer, and PP1 or calcineurin activity was measured using the fluorescence-based RediPlate 96 EnzChek serine/ threonine phosphatase assay kit (Molecular Probes).

Immunohistochemistry

Animals were transcardially perfused with 4% paraformaldehyde in PBS under anesthesia (2:1 of ketamine/xylazine), and brains were sectioned at 40 mm thickness with a Leica VT1000S vibratome (Leica). Slices were permeabilized with blocking solution containing 0.1% Triton X-100, 10% donkey serum, and 2% BSA in PBS for 1 hr at room temperature, and then incubated with indicated antibodies overnight at 4°C. The following day, slices were incubated with fluorescently conjugated secondary antibodies (Molecular Probes) for 1 hr at room temperature, and nuclei were stained with Hoechst 33342 (Invitrogen).

ELISA

Hippocampi were isolated from 7- to 9-month-old females, lysed with 5 M guanidine/50 mM Tris HCl (pH 8.0) buffer, and subjected to Aβ measurement with the use of a human $Aβ_{42}$ or $Aβ_{40}$ ELISA kit (Invitrogen) according to the manufacturer's instructions.

Behavioral Experiments

For behavioral analysis of Δp35KI and WT mice, we used 8-week-old males. For analysis of WT, 5XFAD, Δp35KI, and 5XFAD;Δp35KI mice, we used 6- to 7-month-old males. Mice were handled more than 3 days before each behavioral test.

Electrophysiology

For analysis of Δp35KI mice and their WT littermates, we used 2- to 3-week-old males for LTD experiments, and 3- to 4-week-old males for LTP or intracellular recordings. We used 6- to 7-month-old males for analysis of WT, 5XFAD, Δp35KI, and 5XFAD;Δp35KI mice.

Statistics

Statistical analyses were performed using JMP Pro 10. ANOVAs followed by Tukey's post hoc analyses or unpaired Student's t tests were used. All data are represented as mean ± SEM.

Supplementary Material

Refer to Web version on PubMed Central for supplementary material.

ACKNOWLEDGMENTS

We thank R. Neve for packaging the recombinant herpes simplex viruses; J. Giraud and E. Cornejo for early observations; Z. Xie for assistance in developing the cloning strategy to generate the Δp35KI mouse; W. Xu, S. Su, A. Nott, and A. Bero for helpful comments on the manuscript; and members of the Tsai lab for fruitful advice and discussions. We also thank M. Taylor for animal maintenance. This work was partially supported by the National Institutes of Health (grants R01 NS051874 to L.-H.T. and F31GM80055-03 to P.G.-R.) and the Howard Hughes Medical Institute.

REFERENCES

Angelo M, Plattner F, Irvine EE, Giese KP. Improved reversal learning and altered fear conditioning in transgenic mice with regionally restricted p25 expression. Eur. J. Neurosci. 2003; 18:423–431. [PubMed: 12887424]

Bibb JA, Snyder GL, Nishi A, Yan Z, Meijer L, Fienberg AA, Tsai LH, Kwon YT, Girault JA, Czernik AJ, et al. Phosphorylation of DARPP-32 by Cdk5 modulates dopamine signalling in neurons. Nature. 1999; 402:669–671. [PubMed: 10604473]

Buckner RL, Snyder AZ, Shannon BJ, LaRossa G, Sachs R, Fotenos AF, Sheline YI, Klunk WE, Mathis CA, Morris JC, Mintun MA. Molecular, structural, and functional characterization of Alzheimer's disease: evidence for a relationship between default activity, amyloid, and memory. J. Neurosci. 2005; 25:7709–7717. [PubMed: 16120771]

Carlin RK, Grab DJ, Cohen RS, Siekevitz P. Isolation and characterization of postsynaptic densities from various brain regions: enrichment of different types of postsynaptic densities. J. Cell Biol. 1980; 86:831–845. [PubMed: 7410481]

Chae T, Kwon YT, Bronson R, Dikkes P, Li E, Tsai LH. Mice lacking p35, a neuronal specific activator of Cdk5, display cortical lamination defects, seizures, and adult lethality. Neuron. 1997; 18:29–42. [PubMed: 9010203]

Chen R, Zhang J, Wu Y, Wang D, Feng G, Tang Y-P, Teng Z, Chen C. Monoacylglycerol lipase is a therapeutic target for Alzheimer's disease. Cell Rep. 2012; 2:1329–1339. [PubMed: 23122958]

Cirrito JR, Yamada KA, Finn MB, Sloviter RS, Bales KR, May PC, Schoepp DD, Paul SM, Mennerick S, Holtzman DM. Synaptic activity regulates interstitial fluid amyloid-beta levels in vivo. Neuron. 2005; 48:913–922. [PubMed: 16364896]

Collingridge GL, Isaac JTR, Wang YT. Receptor trafficking and synaptic plasticity. Nat. Rev. Neurosci. 2004; 5:952–962. [PubMed: 15550950]

Crews L, Patrick C, Adame A, Rockenstein E, Masliah E. Modulation of aberrant CDK5 signaling rescues impaired neurogenesis in models of Alzheimer's disease. Cell Death Dis. 2011; 2:e120. [PubMed: 21368891]

Cruz JC, Tseng H-C, Goldman JA, Shih H, Tsai L-H. Aberrant Cdk5 activation by p25 triggers pathological events leading to neurode-generation and neurofibrillary tangles. Neuron. 2003; 40:471–483. [PubMed: 14642273]

Cruz JC, Kim D, Moy LY, Dobbin MM, Sun X, Bronson RT, Tsai L-H. p25/cyclin-dependent kinase 5 induces production and intraneuronal accumulation of amyloid beta in vivo. J. Neurosci. 2006; 26:10536–10541. [PubMed: 17035538]

D'Amelio M, Cavallucci V, Middei S, Marchetti C, Pacioni S, Ferri A, Diamantini A, De Zio D, Carrara P, Battistini L, et al. Caspase-3 triggers early synaptic dysfunction in a mouse model of Alzheimer's disease. Nat. Neurosci. 2011; 14:69–76. [PubMed: 21151119]

Dalton GL, Wang YT, Floresco SB, Phillips AG. Disruption of AMPA receptor endocytosis impairs the extinction, but not acquisition of learned fear. Neuropsychopharmacology. 2008; 33:2416–2426. [PubMed: 18046303]

Dhavan R, Greer PL, Morabito MA, Orlando LR, Tsai L-H. The cyclin-dependent kinase 5 activators p35 and p39 interact with the alpha-subunit of Ca2+/calmodulin-dependent protein kinase II and alpha-actinin-1 in a calcium-dependent manner. J. Neurosci. 2002; 22:7879–7891. [PubMed: 12223541]

Engmann O, Hortobágyi T, Thompson AJ, Guadagno J, Troakes C, Soriano S, Al-Sarraj S, Kim Y, Giese KP. Cyclin-dependent kinase 5 activator p25 is generated during memory formation and is reduced at an early stage in Alzheimer's disease. Biol. Psychiatry. 2011; 70:159–168. [PubMed: 21616478]

Etkin A, Alarcón JM, Weisberg SP, Touzani K, Huang YY, Nordheim A, Kandel ER. A role in learning for SRF: deletion in the adult fore-brain disrupts LTD and the formation of an immediate memory of a novel context. Neuron. 2006; 50:127–143. [PubMed: 16600861]

Fu W-Y, Chen Y, Sahin M, Zhao X-S, Shi L, Bikoff JB, Lai K-O, Yung W-H, Fu AKY, Greenberg ME, Ip NY. Cdk5 regulates EphA4-mediated dendritic spine retraction through an ephexin1-dependent mechanism. Nat. Neurosci. 2007; 10:67–76. [PubMed: 17143272]

Gilmore EC, Ohshima T, Goffinet AM, Kulkarni AB, Herrup K. Cyclin-dependent kinase 5-deficient mice demonstrate novel developmental arrest in cerebral cortex. J. Neurosci. 1998; 18:6370–6377. [PubMed: 9698328]

Gräff J, Rei D, Guan J-S, Wang W-Y, Seo J, Hennig KM, Nieland TJF, Fass DM, Kao PF, Kahn M, et al. An epigenetic blockade of cognitive functions in the neurodegenerating brain. Nature. 2012; 483:222–226. [PubMed: 22388814]

Guan J-S, Haggarty SJ, Giacometti E, Dannenberg J-H, Joseph N, Gao J, Nieland TJF, Zhou Y, Wang X, Mazitschek R, et al. HDAC2 negatively regulates memory formation and synaptic plasticity. Nature. 2009; 459:55–60. [PubMed: 19424149]

Guan J-S, Su SC, Gao J, Joseph N, Xie Z, Zhou Y, Durak O, Zhang L, Zhu JJ, Clauser KR, et al. Cdk5 is required for memory function and hippocampal plasticity via the cAMP signaling pathway. PLoS ONE. 2011; 6:e25735. [PubMed: 21984943]

Halpain S, Girault JA, Greengard P. Activation of NMDA receptors induces dephosphorylation of DARPP-32 in rat striatal slices. Nature. 1990; 343:369–372. [PubMed: 2153935]

Hemmings HC Jr. Greengard P, Tung HY, Cohen P. DARPP-32, a dopamine-regulated neuronal phosphoprotein, is a potent inhibitor of protein phosphatase-1. Nature. 1984; 310:503–505. [PubMed: 6087160]

Jawhar S, Trawicka A, Jenneckens C, Bayer TA, Wirths O. Motor deficits, neuron loss, and reduced anxiety coinciding with axonal degeneration and intraneuronal Ab aggregation in the 5XFAD mouse model of Alzheimer's disease. Neurobiol. Aging. 2012; 33:196.e29–40. [PubMed: 20619937]

Kamenetz F, Tomita T, Hsieh H, Seabrook G, Borchelt D, Iwatsubo T, Sisodia S, Malinow R. APP processing and synaptic function. Neuron. 2003; 37:925–937. [PubMed: 12670422]

Kesavapany S, Zheng Y-L, Amin N, Pant HC. Peptides derived from Cdk5 activator p35, specifically inhibit deregulated activity of Cdk5. Biotechnol. J. 2007; 2:978–987. [PubMed: 17526058]

Kim SH, Ryan TA. CDK5 serves as a major control point in neurotransmitter release. Neuron. 2010; 67:797–809. [PubMed: 20826311]

Kim Y, Sung JY, Ceglia I, Lee K-W, Ahn J-H, Halford JM, Kim AM, Kwak SP, Park JB, Ho Ryu S, et al. Phosphorylation of WAVE1 regulates actin polymerization and dendritic spine morphology. Nature. 2006; 442:814–817. [PubMed: 16862120]

Kim J, Lee S, Park K, Hong I, Song B, Son G, Park H, Kim WR, Park E, Choe HK, et al. Amygdala depotentiation and fear extinction. Proc. Natl. Acad. Sci. USA. 2007; 104:20955–20960. [PubMed: 18165656]

Kimura R, Ohno M. Impairments in remote memory stabilization precede hippocampal synaptic and cognitive failures in 5XFAD Alzheimer mouse model. Neurobiol. Dis. 2009; 33:229–235. [PubMed: 19026746]

Ko J, Humbert S, Bronson RT, Takahashi S, Kulkarni AB, Li E, Tsai LH. p35 and p39 are essential for cyclin-dependent kinase 5 function during neurodevelopment. J. Neurosci. 2001; 21:6758–6771. [PubMed: 11517264]

Kuchibhotla KV, Goldman ST, Lattarulo CR, Wu H-Y, Hyman BT, Bacskai BJ. Abeta plaques lead to aberrant regulation of calcium homeostasis in vivo resulting in structural and functional disruption of neuronal networks. Neuron. 2008; 59:214–225. [PubMed: 18667150]

Lee HK, Kameyama K, Huganir RL, Bear MF. NMDA induces long-term synaptic depression and dephosphorylation of the GluR1 subunit of AMPA receptors in hippocampus. Neuron. 1998; 21:1151–1162. [PubMed: 9856470]

Lee HK, Barbarosie M, Kameyama K, Bear MF, Huganir RL. Regulation of distinct AMPA receptor phosphorylation sites during bidirectional synaptic plasticity. Nature. 2000a; 405:955–959. [PubMed: 10879537]

Lee MS, Kwon YT, Li M, Peng J, Friedlander RM, Tsai LH. Neurotoxicity induces cleavage of p35 to p25 by calpain. Nature. 2000b; 405:360–364. [PubMed: 10830966]

Lee S-H, Choi J-H, Lee N, Lee H-R, Kim J-I, Yu N-K, Choi S-L, Lee S-H, Kim H, Kaang B-K. Synaptic protein degradation underlies destabilization of retrieved fear memory. Science. 2008; 319:1253–1256. [PubMed: 18258863]

Li Z, Jo J, Jia J-M, Lo S-C, Whitcomb DJ, Jiao S, Cho K, Sheng M. Caspase-3 activation via mitochondria is required for long-term depression and AMPA receptor internalization. Cell. 2010; 141:859–871. [PubMed: 20510932]

Li S, Jin M, Koeglsperger T, Shepardson NE, Shankar GM, Selkoe DJ. Soluble Aβ oligomers inhibit long-term potentiation through a mechanism involving excessive activation of extrasynaptic NR2B-containing NMDA receptors. J. Neurosci. 2011; 31:6627–6638. [PubMed: 21543591]

Lu W, Man H, Ju W, Trimble WS, MacDonald JF, Wang YT. Activation of synaptic NMDA receptors induces membrane insertion of new AMPA receptors and LTP in cultured hippocampal neurons. Neuron. 2001; 29:243–254. [PubMed: 11182095]

Mitra A, Mitra SS, Tsien RW. Heterogeneous reallocation of presynaptic efficacy in recurrent excitatory circuits adapting to inactivity. Nat. Neurosci. 2012; 15:250–257. [PubMed: 22179109]

Mukerjee N, McGinnis KM, Park YH, Gnegy ME, Wang KK. Caspase-mediated proteolytic activation of calcineurin in thapsigargin-mediated apoptosis in SH-SY5Y neuroblastoma cells. Arch. Biochem. Biophys. 2000; 379:337–343. [PubMed: 10898953]

Mulkey RM, Herron CE, Malenka RC. An essential role for protein phosphatases in hippocampal long-term depression. Science. 1993; 261:1051–1055. [PubMed: 8394601]

Mulkey RM, Endo S, Shenolikar S, Malenka RC. Involvement of a calcineurin/inhibitor-1 phosphatase cascade in hippocampal long-term depression. Nature. 1994; 369:486–488. [PubMed: 7515479]

Oakley H, Cole SL, Logan S, Maus E, Shao P, Craft J, Guillozet-Bongaarts A, Ohno M, Disterhoft J, Van Eldik L, et al. Intraneuronal beta-amyloid aggregates, neurodegeneration, and neuron loss in transgenic mice with five familial Alzheimer's disease mutations: potential factors in amyloid plaque formation. J. Neurosci. 2006; 26:10129–10140. [PubMed: 17021169]

Ohshima T, Ogura H, Tomizawa K, Hayashi K, Suzuki H, Saito T, Kamei H, Nishi A, Bibb JA, Hisanaga S-I, et al. Impairment of hippocampal long-term depression and defective spatial learning and memory in p35 mice. J. Neurochem. 2005; 94:917–925. [PubMed: 15992381]

Otth C, Concha II, Arendt T, Stieler J, Schliebs R, González-Billault C, Maccioni RB. AbetaPP induces cdk5-dependent tau hyperphosphorylation in transgenic mice Tg2576. J. Alzheimers Dis. 2002; 4:417–430. [PubMed: 12446973]

Patrick GN, Zukerberg L, Nikolic M, de la Monte S, Dikkes P, Tsai LH. Conversion of p35 to p25 deregulates Cdk5 activity and promotes neurodegeneration. Nature. 1999; 402:615–622. [PubMed: 10604467]

Perry VH, Nicoll JAR, Holmes C. Microglia in neurodegenerative disease. Nat. Rev. Neurol. 2010; 6:193–201. [PubMed: 20234358]

Sadleir KR, Vassar R. Cdk5 protein inhibition and Ab42 increase BACE1 protein level in primary neurons by a post-transcriptional mechanism: implications of CDK5 as a therapeutic target for Alzheimer disease. J. Biol. Chem. 2012; 287:7224–7235. [PubMed: 22223639]

Seeburg DP, Feliu-Mojer M, Gaiottino J, Pak DTS, Sheng M. Critical role of CDK5 and Polo-like kinase 2 in homeostatic synaptic plasticity during elevated activity. Neuron. 2008; 58:571–583. [PubMed: 18498738]

Shuai Y, Lu B, Hu Y, Wang L, Sun K, Zhong Y. Forgetting is regulated through Rac activity in Drosophila. Cell. 2010; 140:579–589. [PubMed: 20178749]

Su SC, Tsai L-H. Cyclin-dependent kinases in brain development and disease. Annu. Rev. Cell Dev. Biol. 2011; 27:465–491. [PubMed: 21740229]

Swatton JE, Sellers LA, Faull RLM, Holland A, Iritani S, Bahn S. Increased MAP kinase activity in Alzheimer's and Down syndrome but not in schizophrenia human brain. Eur. J. Neurosci. 2004; 19:2711–2719. [PubMed: 15147305]

Szapiro G, Vianna MRM, McGaugh JL, Medina JH, Izquierdo I. The role of NMDA glutamate receptors, PKA, MAPK, and CAMKII in the hippocampus in extinction of conditioned fear. Hippocampus. 2003; 13:53–58. [PubMed: 12625457]

Tandon A, Yu H, Wang L, Rogaeva E, Sato C, Chishti MA, Kawarai T, Hasegawa H, Chen F, Davies P, et al. Brain levels of CDK5 activator p25 are not increased in Alzheimer's or other neurodegenerative diseases with neurofibrillary tangles. J. Neurochem. 2003; 86:572–581. [PubMed: 12859671]

Tronson NC, Corcoran KA, Jovasevic V, Radulovic J. Fear conditioning and extinction: emotional states encoded by distinct signaling pathways. Trends Neurosci. 2012; 35:145–155. [PubMed: 22118930]

Verkhratsky A, Olabarria M, Noristani HN, Yeh C-Y, Rodriguez JJ. Astrocytes in Alzheimer's disease. Neurotherapeutics. 2010; 7:399–412. [PubMed: 20880504]

Wen Y, Yu WH, Maloney B, Bailey J, Ma J, Marié I, Maurin T, Wang L, Figueroa H, Herman M, et al. Transcriptional regulation of beta-secretase by p25/cdk5 leads to enhanced amyloidogenic processing. Neuron. 2008; 57:680–690. [PubMed: 18341989]

Yang T, Knowles JK, Lu Q, Zhang H, Arancio O, Moore LA, Chang T, Wang Q, Andreasson K, Rajadas J, et al. Small molecule, non-peptide p75 ligands inhibit Abeta-induced neurodegeneration and synaptic impairment. PLoS ONE. 2008; 3:e3604. [PubMed: 18978948]

Yoo BC, Lubec G. p25 protein in neurodegeneration. Nature. 2001; 411:763–764. discussion 764–765. [PubMed: 11459045]

Zhang M, Storm DR, Wang H. Bidirectional synaptic plasticity and spatial memory flexibility require Ca2+-stimulated adenylyl cyclases. J. Neurosci. 2011; 31:10174–10183. [PubMed: 21752993]

Zhao J, Fu Y, Yasvoina M, Shao P, Hitt B, O'Connor T, Logan S, Maus E, Citron M, Berry R, et al. Beta-site amyloid precursor protein cleaving enzyme 1 levels become elevated in neurons around amyloid plaques: implications for Alzheimer's disease pathogenesis. J. Neurosci. 2007; 27:3639–3649. [PubMed: 17409228]

Zukerberg LR, Patrick GN, Nikolic M, Humbert S, Wu CL, Lanier LM, Gertler FB, Vidal M, Van Etten RA, Tsai LH. Cables links Cdk5 and c-Abl and facilitates Cdk5 tyrosine phosphorylation, kinase upregulation, and neurite outgrowth. Neuron. 2000; 26:633–646. [PubMed: 10896159]

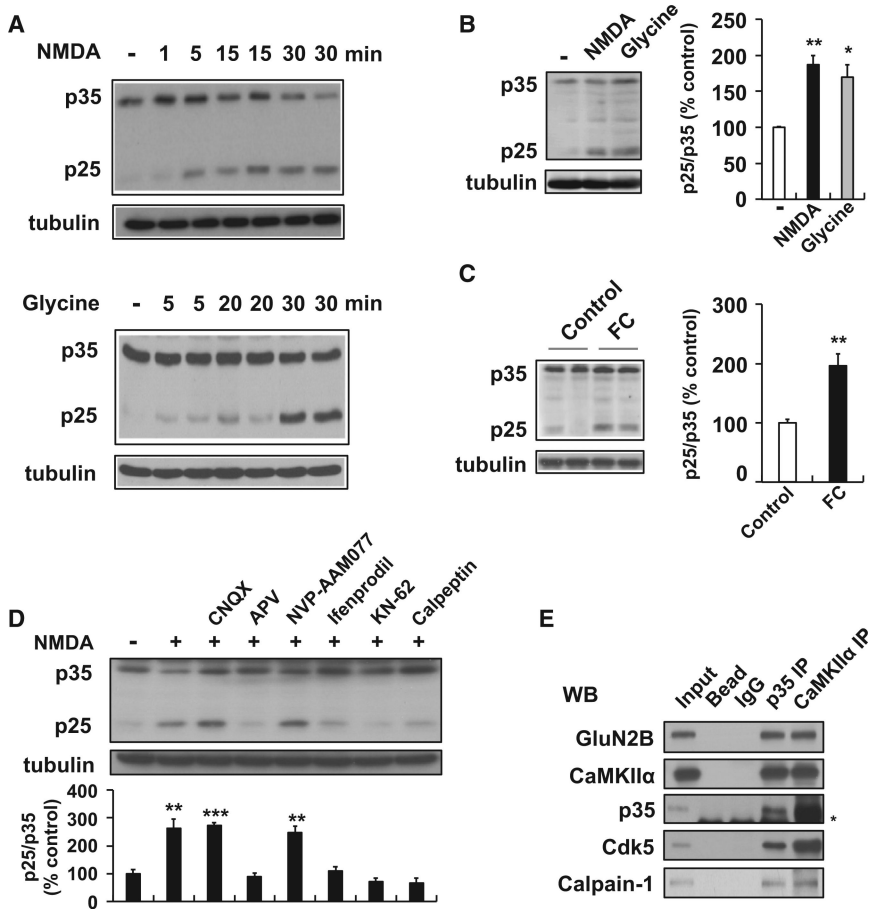

Figure 1. Activity-Induced p25 Generation in Hippocampus via NMDAR and CaMKIIα

(A) Primary cultured neurons were treated with NMDA (100 μM for 5 min) or glycine (200 μM for 3 min), and further incubated in conditioned media for the specified times.

(B) Acute hippocampal slices were treated with NMDA (50 μM for 5 min) or glycine (100 μM for 3 min), followed by ACSF for 15 min. Right: the bar graph represents relative immunoreactivity of p25/ p35 compared with control (n = 3 per group).

(C) WT mice were sacrificed after contextual FC (0.8 mA shock for 2 s) and hippocampi were isolated for immunoblotting (n = 6 per group).

(D) Pretreatment of hippocampal slices with the AMPAR antagonist CNQX (10 μM), the NMDAR antagonist APV (50 μM), the GluN2A subunit-specific inhibitor NVP-AAM077 (0.5 μM), the GluN2B subunit-specific inhibitor ifenprodil (10 μM), the CaMKIIα inhibitor KN-62 (10 μM), or the calpain inhibitor calpeptin (10 μM) followed by NMDA treatment (n = 3–4 per group).

(E) PSD fractions from WT hippocampus were subjected to the IP with an anti-p35 or anti-CaMKIIα antibody. The asterisk represents a nonspecific background band. *p < 0.05, **p < 0.01, ***p < 0.001 by Student's t test; error bars ± SEM. See also Figure S1.

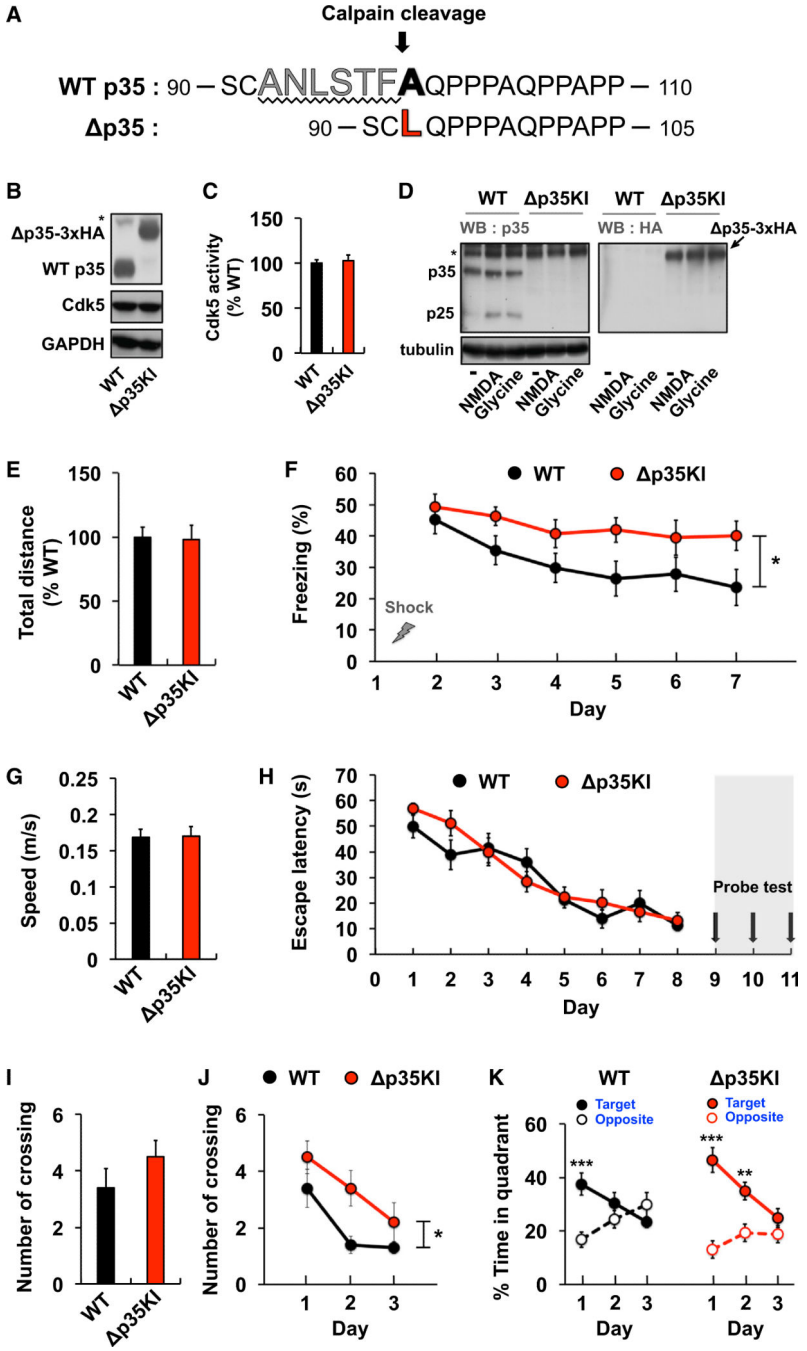

Figure 2. Normal Learning but Impaired Memory Extinction in Δp35KI Mice

(A) Strategy for generating the calpain-mediated, cleavage-resistant p35 protein.

(B) Expression levels of p35 and Δp35 in the fore-brain of WT and Δp35KI mice, respectively. The asterisk represents a nonspecific background band.

(C) IP-linked Cdk5 kinase assay was performed on WT or Δp35KI brain lysates and normalized to WT (n = 4 per group).

(D) p25 expression in WT and Δp35KI hippocampal slices following NMDA or glycine treatment. Δp35 expression in Δp35KI hippocampus was confirmed by immunoblotting with an anti-HA antibody. The asterisk represents a nonspecific background band.
(E) Basal movement behavior of WT (n = 9) and Δp35KI (n = 8) mice during the habituation period before FC.
(F) Fear memory extinction testing by daily re-exposure to the conditioning chamber (repeated-measures ANOVA).
(G) Swim speeds of WT (n = 10) and Δp35KI (n = 10) mice during the water maze test.
(H) Escape latencies of WT and Δp35KI mice in the Morris water maze test.
(I) Number of platform crossings by WT and Δp35KI mice on the first probe test day.
(J) Number of platform crossings by WT and Δp35KI mice during repeated probe trials (repeated-measures ANOVA).
(K) Time spent by WT and Δp35KI mice in the target or the opposite quadrant during repeated probe trials (Student's t test). *$p < 0.05$; **$p < 0.01$; ***$p < 0.001$; error bars ± SEM. See also Figures S2 and S3.

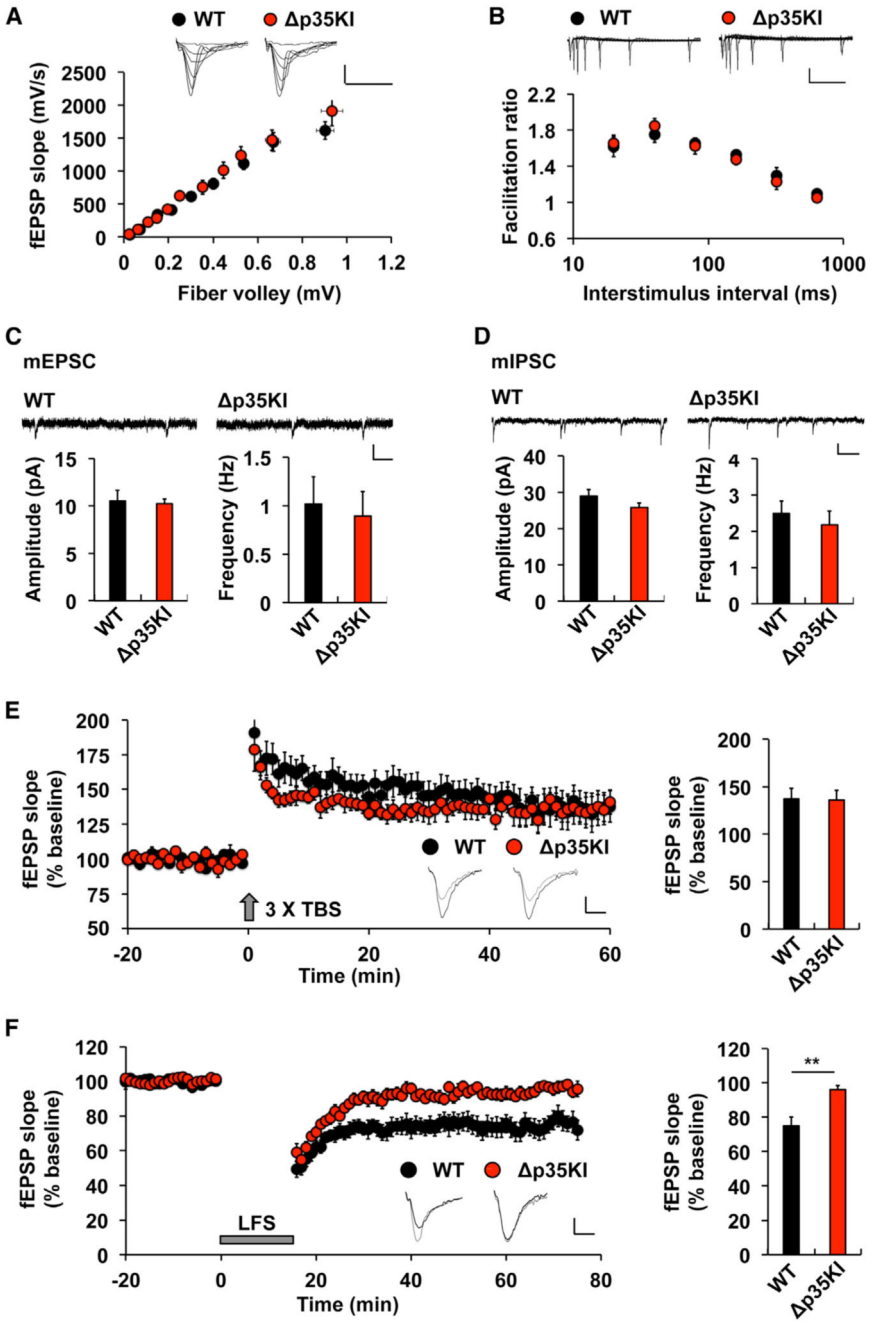

Figure 3. Normal Synaptic Transmission and LTP, but Impaired LTD, in Δp35KI Hippocampus

(A) The synaptic input-output relationship was obtained by plotting the slopes of evoked fEPSPs against fiber-volley amplitude. WT, n = 7 slices from 4 mice; Δp35KI, n = 8 slices from 4 mice. Scale bars, 0.5 mV and 20 ms.

(B) The ratios of paired-pulse facilitation (second fEPSP slope/first fEPSP slope) were plotted as a function of interstimulus interval (ms). WT, n = 6 slices from 3 mice; Δp35KI, n = 5 slices from 3 mice. Scale bars, 0.5 mV and 200 ms.

(C) mEPSC amplitude and frequency in CA1 pyramidal neurons of WT and Δp35KI mice (WT, amplitude: 10.5% ± 1.1%, frequency: 1.0% ± 0.3%, 12 slices from 3 mice; Δp35KI,

amplitude: 10.2% ± 0.5%, frequency: 0.90% ± 0.3%, 11 slices from 3 mice). Scale bars, 10 pA and 200 ms.

(D) mIPSC amplitude and frequency in CA1 pyramidal neurons of WT and Δp35KI mice (WT, amplitude: 29.0% ± 1.8%, frequency: 2.5% ± 0.3%, 13 slices from 3 mice; Δp35KI, amplitude: 25.9% ± 1.3%, frequency: 2.2% ± 0.4%, 11 slices from 3 mice). Scale bars, 10 pA and 200 ms.

(E) LTP was induced by 33 TBS at the Schaffer collateral-CA1 synapses of WT or Δp35KI mice. Sample traces represent fEPSPs at 1 min before (gray) and 1 hr after (black) TBS. Scale bars, 0.5 mV and 10 ms. Right: the magnitude of LTP was calculated by comparing the average slopes of fEPSPs during the last 10 min of recordings with those recorded before stimulation (WT: 137.3% ± 11.2%, 9 slices from 4 mice; Δp35KI: 136.1% ± 10.0%, 6 slices from 3 mice).

(F) LTD was induced by SP-LFS at the Schaffer collateral-CA1 synapses of WT or Δp35KI mice. Sample traces represent fEPSPs at 1 min before (gray) and 1 hr after (black) SP-LFS. Scale bars, 0.5 mV and 10 ms. Right: the magnitude of LTD was calculated by comparing the average slopes of fEPSPs during the last 10 min of recordings with those recorded before stimulation (WT: 75.0% ± 5.3%, 7 slices from 4 mice; Δp35KI: 96.1% ± 2.3%, 8 slices from 4 mice).

**$p < 0.01$ by Student's t test; error bars ± SEM. See also Figure S4.

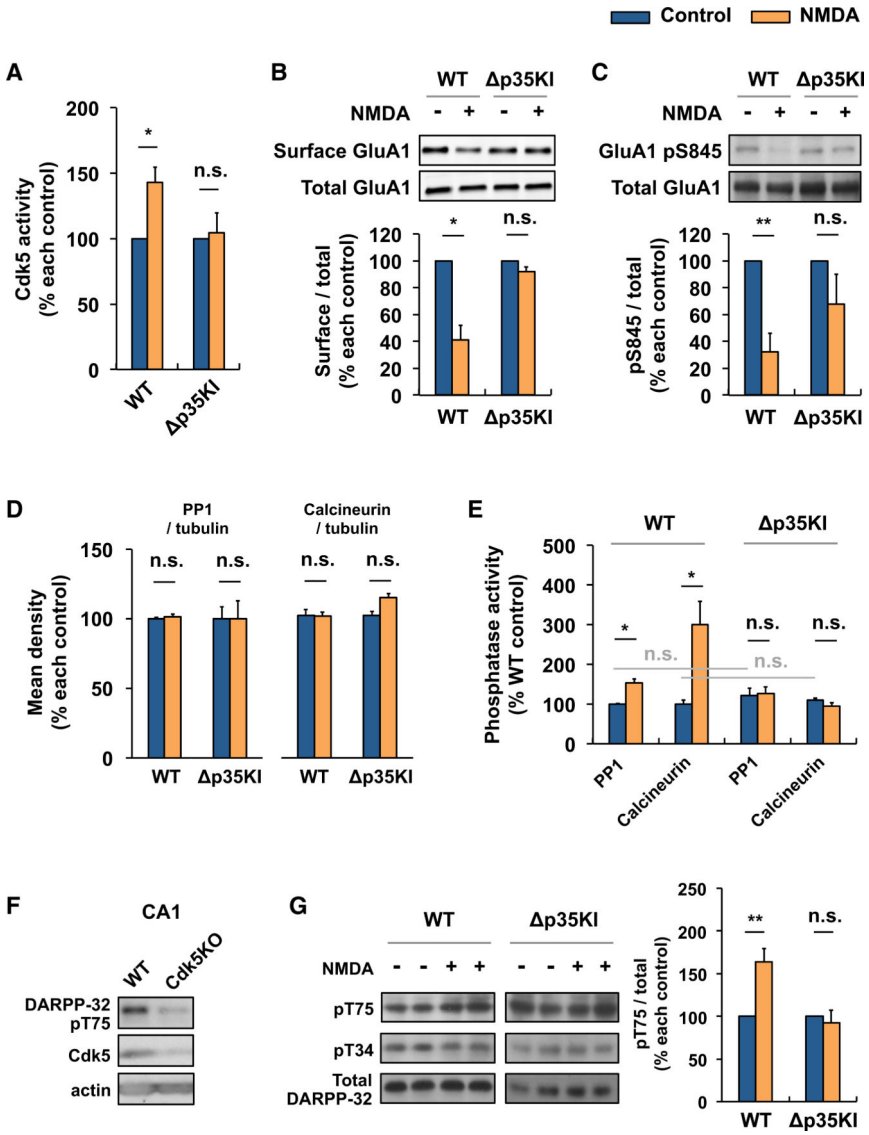

Figure 4. p25/Cdk5 Mediates NMDA-Induced AMPAR Endocytosis by Inhibiting DARPP-32 and Activating PP1 and Calcineurin at Hippocampal Synapses

(A) NMDA was applied to acute hippocampal slices for 5 min, followed by ACSF for an additional 5 min. Cdk5 kinase assay was performed on WT or Δp35KI hippocampal lysates, and Cdk5 activity was normalized to each untreated control (n = 4 per group).

(B) NMDA was applied to acute hippocampal slices and the slices were then allowed to recover for 30 min. Biotinylation assay was performed to measure surface/total levels of GluA1. Bottom: the relative immunoreactivity of surface GluA1/total GluA1 levels were normalized to each untreated control (n = 3 per group).

(C) NMDA was applied to acute hippocampal slices and the slices were allowed to recover for 15 min before being lysed for immunoblotting. Bottom: the relative immunoreactivity of GluA1 pSer845/total GluA1 was normalized to each untreated control (n = 6 per group).

(D) The expression levels of PP1 and calcineurin before and after NMDA treatment were examined by immunoblotting, and relative immunoreactivity of PP1 or calcineurin was normalized to each untreated control (n = 3 per group).
(E) NMDA was applied to acute hippocampal slices and the slices were allowed to recover for 5 min. Protein phosphatase assays were performed on WT or Δp35KI hippocampal lysates, and PP1 and calcineurin activity was normalized to WT control (n = 3 per group).
(F) Immunoblot analysis was performed with an anti-DARPP-32 pThr75 antibody using the lysates from hippocampal CA1 of Cdk5f/f/T29 mice. An anti-Cdk5 antibody was used for confirmation of Cdk5 knockout.
(G) NMDA was applied to acute hippocampal slices and the slices were allowed to recover for 5 min before being lysed for immunoblotting. Right: the relative immunoreactivity of DARPP-32 pThr75/total DARPP-32 was normalized to each control (n = 4 per group).
*p < 0.05, **p < 0.01 by Student's t test; error bars ± SEM. See also Figure S4.

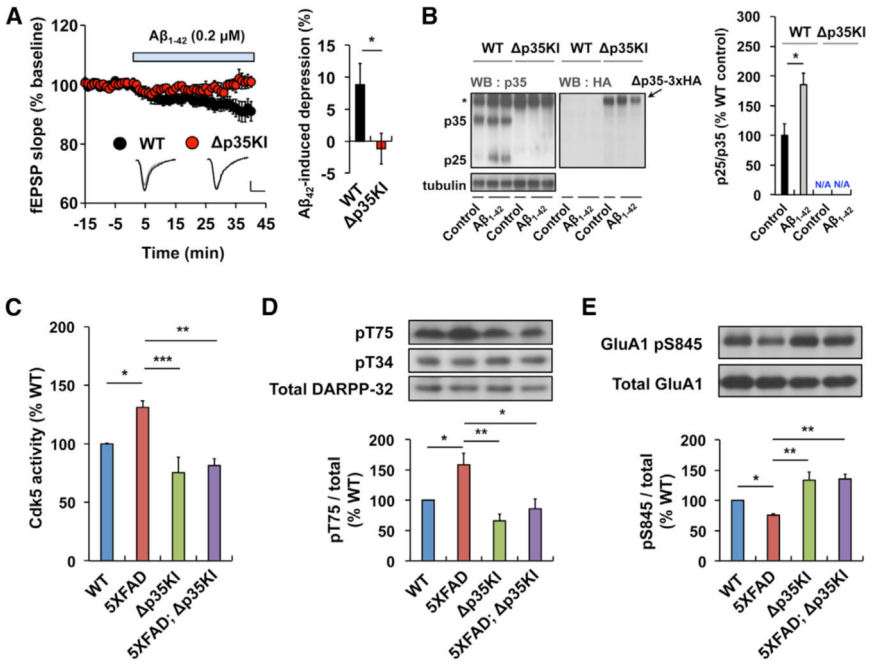

Figure 5. Prevention of Aβ-Induced Synaptic Depression and Excessive DARPP-32 Inhibition and AMPAR Dephosphorylation in 5XFAD Mouse Brain by Blockade of p25 Generation

(A) Stable basal synaptic transmission was recorded from WT or Δp35KI hippocampal slices for at least 15 min, followed by incubation in $A\beta_{1\text{-}42}$ (0.2 μM) for 40 min. Scale bars, 0.5 mV and 10 ms. Sample traces represent fEPSPs at 1 min before (gray) and 40 min after (black) $A\beta_{1\text{-}42}$ treatment. Right: the magnitude of $A\beta_{1\text{-}42}$-induced depression was calculated by comparing the average slopes of fEPSPs during the last 10 min of recordings with those obtained before $A\beta_{1\text{-}42}$ treatment (WT: 8.8%± 3.3%, 7 slices from 3 mice; Δp35KI: 1.2% ± 2.4%, 6 slices from 3 mice). Student's t test.

(B) Levels of p25 in WT and Δp35KI hippocampus after incubation with $A\beta_{1\text{-}42}$. Δp35 expression in Δp35KI hippocampus was confirmed by immunoblotting with an anti-HA antibody. The asterisk represents a nonspecific background band. Right: the bar graph represents relative immunoreactivity of p25/p35 compared with the WT untreated group (n = 5 per group; Student's t test).

(C) IP-linked Cdk5 kinase assays were performed on WT, 5XFAD, Δp35KI, or 5XFAD;Δp35KI hippocampal lysates (n = 5 per group).

(D) The relative immunoreactivity of DARPP-32 pThr75/total DARPP-32 was normalized to WT (n = 4–6 per group; $p < 0.01$ by ANOVA).

(E) The relative immunoreactivity of GluA1 pSer845/total GluA1 was normalized to WT (n = 3 per group; $p < 0.01$ by ANOVA). *$p < 0.05$, **$p < 0.01$, ***$p < 0.001$ by Student's t test or Tukey's post hoc analysis; error bars ± SEM. See also Figure S5.

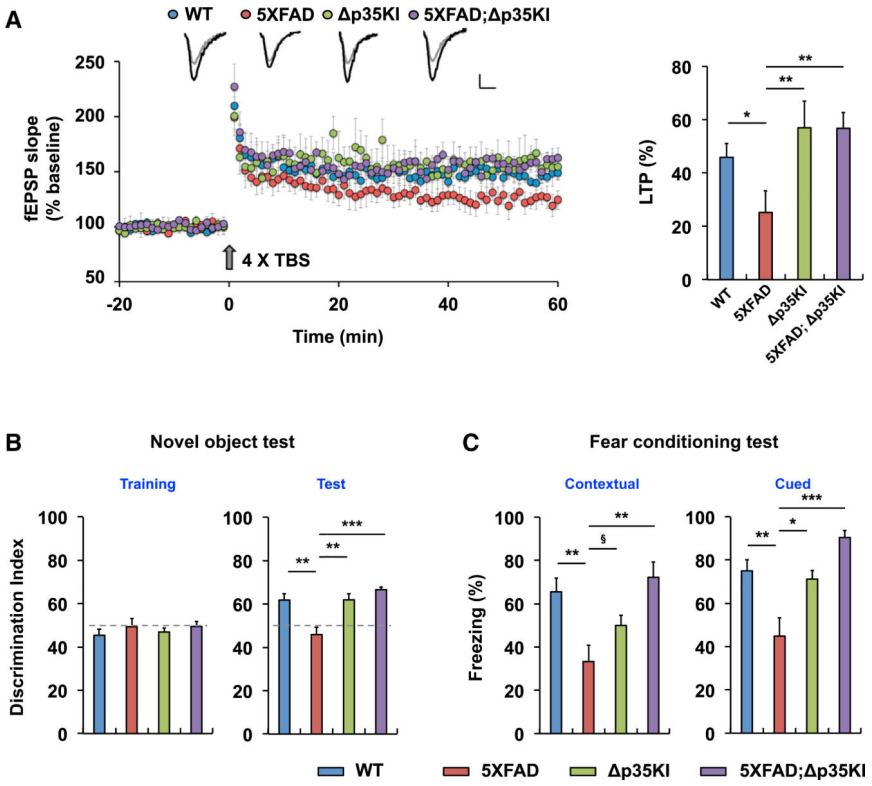

Figure 6. Inhibition of p25 Generation Rescues Synaptic Dysfunction and Cognitive Impairment in 5XFAD Mice

(A) LTP was induced by 4× TBS at Schaffer collateral-CA1 synapses. Sample traces represent fEPSPs at 1 min before (gray) and 1 hr after (black) TBS. Scale bars, 0.5 mV and 10 ms. Right: the magnitude of LTP was calculated by comparing the average slopes of fEPSPs during the last 10 min of recordings with those recorded before stimulation. WT: 146.0% ± 5.1%, 8 slices from 5 mice; 5XFAD: 125.2% ± 8.1%, 7 slices from 5 mice; Δp35KI: 157.0% ± 10.1%, 5 slices from 3 mice; 5XFAD;Δp35KI: 156.8% ± 5.9%, 5 slices from 3 mice, $p < 0.01$ by ANOVA.

(B) Novel-object test with WT, Δp35KI, 5XFAD, and 5XFAD;Δp35KI mice. Right: discrimination index for novel-object recognition (WT: 61.8 ± 2.8, n = 8; 5XFAD: 45.9 ± 3.5, n = 7; Δp35KI: 61.9 ± 2.8, n = 6; 5XFAD;Δp35KI: 66.6 ± 1.3, n = 9, $p < 0.001$ by ANOVA).

(C) Contextual and cued FC tests with WT, Δp35KI, 5XFAD, and 5XFAD;Δp35KI mice. Left: contextual FC (WT: 65.6% ± 6.4%, n = 10; 5XFAD: 33.3% ± 7.6%, n = 12; Δp35KI: 50.0% ± 4.7%, n = 11; 5XFAD;Δp35KI: 72.2% ± 7.0%, n = 7, $p < 0.05$ by ANOVA). Right: cued FC (WT: 75.0% ± 5.0%, n = 10; 5XFAD: 44.9% ± 8.3%, n = 12; Δp35KI: 71.2% ± 3.9%, n = 11; 5XFAD;Δp35KI: 90.5% ± 3.1%, n = 7, $p < 0.01$ by ANOVA).

§p = 0.08, *p < 0.05, **p < 0.01, ***p < 0.001 by Tukey's post hoc analysis; error bars ± SEM. See also Figure S6.

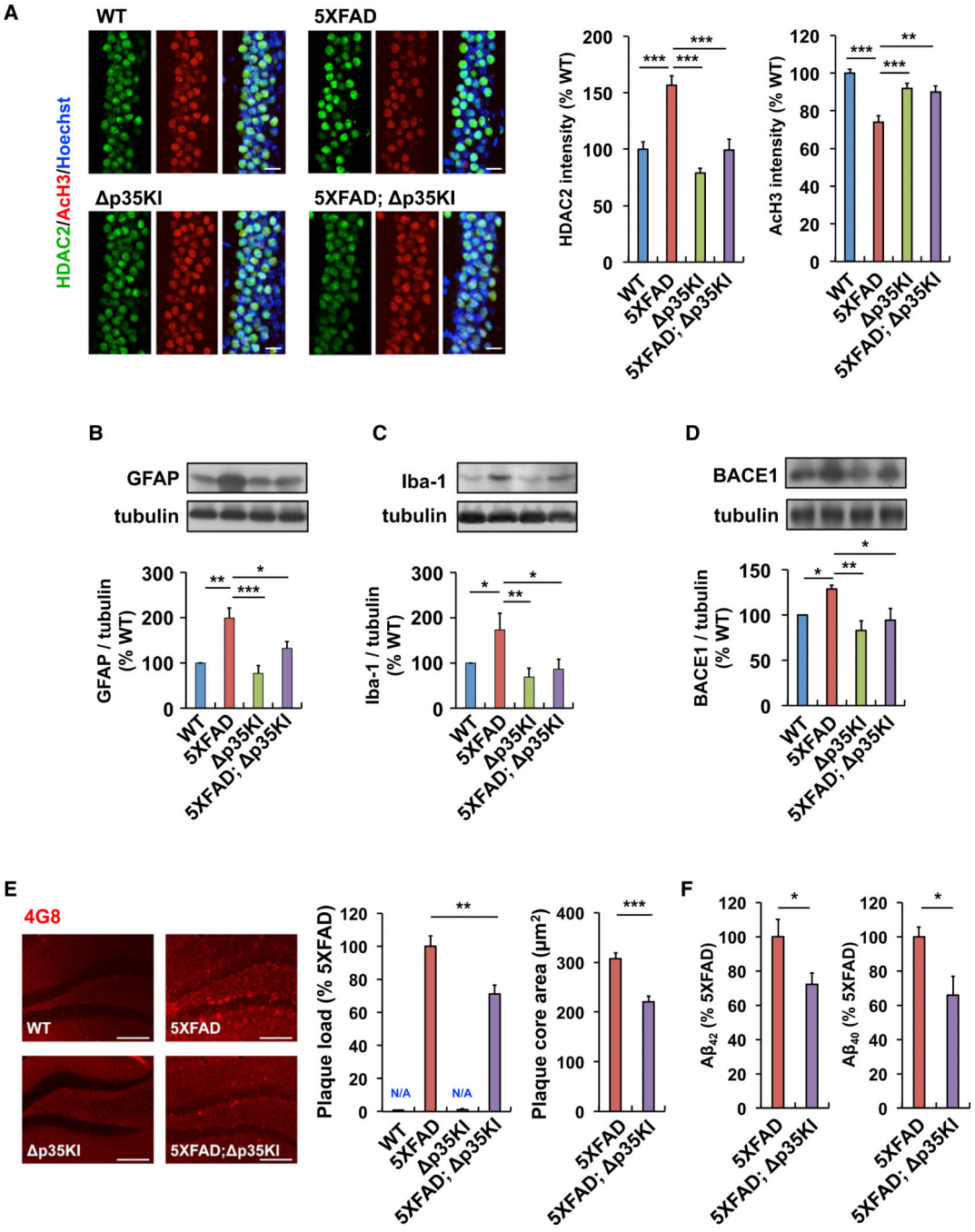

Figure 7. Inhibition of p25 Generation Attenuates Elevated HDAC2 Levels, Glial Activation, and Aβ Accumulation in 5XFAD Mice

(A) Immunohistochemistry with anti-HDAC2 and anti-acetylated H3K9/14 (AcH3) antibodies in hippocampal CA1 of WT, Δp35KI, 5XFAD, and 5XFAD;Δp35KI mice. Scale bar, 20 μm. Right: bar graphs represent the relative immunoreactivity of HDAC2 and AcH3 normalized to WT (n = 10–14 slices from 3 mice per group; $p < 0.001$ by ANOVA).

(B) Relative immunoreactivity of GFAP in hippocampus of WT, Δp35KI, 5XFAD, and 5XFAD;Δp35KI mice normalized to WT (n = 4 per group; $p < 0.001$ by ANOVA).

(C) Relative immunoreactivity of Iba-1 in the hippocampus of WT, Δp35KI, 5XFAD, and 5XFAD;Δp35KI mice normalized to WT (n = 4 per group; $p < 0.05$ by ANOVA).
(D) Relative immunoreactivity of BACE1 in the hippocampus of WT, Δp35KI, 5XFAD, and 5XFAD;Δp35KI mice normalized to WT (n = 5 per group; $p < 0.05$ by ANOVA).
(E) Immunohistochemistry with an anti-4G8 antibody in hippocampal CA1 of WT, Δp35KI, 5XFAD, and 5XFAD;Δp35KI mice. Scale bar, 100 mm. Middle: the number of Aβ plaques/mm^2 in hippocampus was quantified and normalized to 5XFAD mice. Right: the size of Aβ plaques was measured and normalized to 5XFAD mice (n = 21–24 slices from 7 mice per group; Student's t test).
(F) Hippocampal $A\beta_{1\text{-}42}$ and $A\beta_{1\text{-}40}$ levels were measured by ELISA and normalized to 5XFAD (n = 6–7 per group for $A\beta_{1\text{-}42}$, and n = 3 per group for $A\beta_{1\text{-}40}$ measurement; Student's t test). *$p < 0.05$, **$p < 0.01$, ***$p < 0.001$ by Student's t test or Tukey's post hoc analysis; error bars ± SEM. See also Figure S7.